World Academy of Science, Engineering and Technology
International Journal of Mechanical and Mechatronics Engineering
Vol:13, No:3, 2019

Shear Layer Investigation through a High-Load Cascade in Low-Pressure Gas Turbine Conditions

Mehdi Habibnia Rami, Shidvash Vakilipour, Mohammad H. Sabour, Rouzbeh Riazi, Hossein Hassannia

***Abstract*—**This paper deals with the steady and unsteady flow behavior on the separation bubble occurring on the rear portion of the suction side of T106A blade. The first phase was to implement the steady condition capturing the separation bubble. To accurately predict the separated region, the effects of three different turbulence models and computational grids were separately investigated. The results of Large Eddy Simulation (LES) model on the finest grid structure are acceptably in a good agreement with its relevant experimental results. The second phase is mainly to address the effects of wake entrance on bubble disappearance in unsteady situation. In the current simulations, from what was suggested in an experiment, simulating the flow unsteadiness, with concentrations on small scale disturbances instead of simulating a complete oncoming wake, is the key issue. Subsequently, the results from the current strategy to apply the effects of the wake and two other experimental work were compared to be in a good agreement. Between the two experiments, one of them deals with wake passing unsteady flow, and the other one implements experimentally the same approach as the current Computational Fluid Dynamics (CFD) simulation.

***Keywords*—**T106A turbine cascade, shear-layer separation, steady and unsteady conditions, turbulence models, OpenFOAM.

I. Introduction

IN turbomachinery applications, the advent of high and ultra-high loaded blades in conjunction with steady and unsteady flow behavior resulted in a very challenging pace of work. Applying high engineering attention to promote gas turbine efficiency, coupled with Computational Fluid Dynamics (CFD) capabilities made a remarkable joint in more improvements on the so-called facilities. The most significant part of the low-pressure (LP) turbine relates to the boundary layer behavior and its interaction with the flow free stream in the outer regions, far normal distance through the blades.

In accordance with turbine blade investigations, T106A cascade is the one which is highly recommended amongst LP turbines with its applicability in several engines. Significant energy losses are observed when the flow separates downstream of turbine blade suction side [1]. Due to relative motion of the blade rows, the generated wakes of each blade row are passed to the next one by velocity field. Hence, the presence of the incoming wakes is another important factor in flow and heat transfer characterization within a turbine cascade. Stieger and Hodson [2] investigated transition on the blade suction side by means of Laser Doppler Anemometry (LDA) measurements using cylinders as the wake generators. In another work, they used LDA to measure the turbulent kinetic energy (TKE) production which affects the flow attitude at the rear side of suction surface where the shear layer separation is inevitable [3].

Lodefier and Dick [4] studied the similar case numerically considering the effects of Reynolds numbers using k-ω RANS model. They suggested that, in order to capture the large-scale vortex breakdown in low Reynolds number flows, it is necessary to use a hybrid Reynolds-averaged Navier-Stokes (RANS)/Large Eddy Simulation **(**LES) model. Wissink et al. [5] applied a Direct Numerical Simulation (DNS) model with turbulence intensity (Tu) of 4% to simulate fluctuations of flow field. They showed that large scale disturbance triggers the instability of shear layer along downstream half of the suction side. Opoka et al. [6] showed that the transition on the suction side respond to the free stream velocity changes is motivated by downstream pressure field. Calzada and Alonso [7] studied heat transfer mechanism in separated flows on a low-pressure turbine blade. They demonstrated that, as the Reynolds number increased, the size of separated flow region does not change, the local Stanton number decreases.

Hodson and Dominy [8] investigated the off-design performance of a LP turbine cascade at different inflow incidence angles. They measured the location of separation point by setting the inflow angle to -20.3°, 0° (design point), and +8.6°.

Wu and Durbin [9] performed a DNS of flow structures in T106 turbine passage, considering the initiation of longitudinal vortices. They reported that the longitudinal vortex pairs are not produced by a Görtler instability. They concluded that longitudinal vortex pairs are a forced response to the incident wake, and an adequately accurate prediction of these phenomena leads to more efficiency achievements in turbines applications. Michelassi et al. [10] performed LES calculations of flow around LP turbine blade considering the incoming wakes interactions with the boundary layer.

Matsuura and Kato [11] performed LES of flows around T106 turbine blade. They provided a detailed view of the flow characteristics when the Tu is applied to the free-stream. Through their considerations, the presence of Tu leads to a remarkable reduction of the pressure wakes propagation.

M. Habibnia Rami is MSc student of the Faculty of New Sciences and Technologies, University of Tehran, Tehran, Iran, (corresponding author, phone: +98-21-6111-8454; fax: +98-21-8861-7081; e-mail: (m.habibnia@ut.ac.ir).

S. Vakilipour is with the Faculty of New Sciences and Technologies, University of Tehran, Tehran, Iran, (e-mail: vakilipour@ut.ac.ir).

M. H. Sabour is with the Faculty of New Sciences and Technologies, University of Tehran, Tehran, Iran, (e-mail: sabourmh@ut.ac.ir).

R. Riazi is with the Faculty of New Sciences and Technologies, University of Tehran, Tehran, Iran (email: ro_riazi@ut.ac.ir).

H. Hassannia is MSc student of the Faculty of Mechanical Engineering, of Ayatollah Amoli Azad University (email: hasannia.hosein@gmail.com).

Reversely, the absence of the free-stream Tu results in unsteady fluctuations of the mentioned wakes on the suction side downstream in separation region. Velez et al. [12] presented a comparison between LES, scale adaptive simulation (SAS), shear stress transport (SST), Spalart-Allmaras (SA), and k-ε models. Among all mentioned turbulence models, they showed that LES is the most appropriate model that would be able to predict the flow patterns such as transition.

Ghidoni et al. [13] implemented a high-order accurate discontinuous Galerkin (DG) method for the simulation of transitional flow passing through T106A turbine cascade. The main feature of their work was inclusion of both the high and low Reynolds turbulence models. Their DG method showed an acceptable and efficient modelling of boundary layer transition and reattachment even on a coarse grid.

Amongst the three main transition mechanisms which were observed and proposed by Mayle [14], two of them are considered in T106A LP turbine cascade. In the case of steady state flow, the transition type goes to the one named *separation-Induced* transition. As documented in [6] and [15], in steady measurements, the presence of a vast separation bubble is dominant on the downstream portion of the suction surface of the blade. The other transition type named *bypass* transition occurs whenever the flow is disturbed by large fluctuations in the outer region of the shear layer.

The shear layer behavior has been investigated in detail on T106A LP turbine passage using CFD approach in OpenFOAM platform. On the suction side, the flow prediction is highly sensitive to a wide variety of parameters like Reynolds (Re) number, accelerating-decelerating rate of the flow velocity, free stream turbulence intensity, grid size, resolution, and so on. Although the presence of a laminar separation bubble is inevitable in steady measurements, the entrance of unsteadiness to the cascade flow, when interacting with adjacent rows, frequently damps the bubble generation. As a matter of fact, the flow energy decays considerably when a large distance of blade length is covered by a separated flow layer [1].

The present study deals with the numerical investigation of the grid resolution and turbulence models effects on pressure distribution over the LP turbine T106 blade surfaces. Grids "1", "2", and "3" are generated by quadrilateral elements for flow calculation which include 25,000 and 42,000 and 139,000 cells, respectively. The numerical computation is performed using OpenFOAM CFD toolbox which was originally developed as C++ library classes for a broad range of fluid dynamics applications [16]. The computations have been performed with both steady-state and unsteady time marching algorithms using k-ε and k-ω RANS models with the aim of a further interpretation of flow characteristics around this typical LP turbine blade.

II. T106A Turbine Blade

The chosen test case in the present study refers to a new type of blade generation as highly-loaded, since they operate under intense force loading compared to their conventional peers [17]. Moreover, T106A blade belongs to the aft-load category, since the position of maximum and minimum pressure extremes are located on the second half of the blade axial chord.

The base form of these geometries called T106 cascade was firstly reported by Hoheisel [18] and was officially published as a test case in AGARD-AR-275. From these initial reports, T106 cascade was then categorized to numerous types by subsequent numerical and experimental researchers towards their applicability in different working conditions in turbomachinery environment. The first numerical study on the current blade backs to Hildebrandt and Fottner [19] in 1999. Fig. 1 reveals a typical configuration of the so called T106A blade profile, and the substantial flow specifications through this LP turbine cascade are demonstrated in Table I.

TABLE I
T106A Blade Geometry and Flow Specifications

Parameter	Symbol	Value
Blade chord	L	198 mm
Axial blade chord	C_{AX}	170 mm
Reynolds number	Re	1.6×105
Exit Isentropic Mach Number	M_{2is}	0.59
Turbulence intensity	*Tu*	< 0.5
Inlet flow angle	B_1	127.7°
Outlet flow angle	B_2	26.8°
Stagger angle	B_S	52.3°
Cascade pitch	S_c	--
Bar pitch	S_b	--

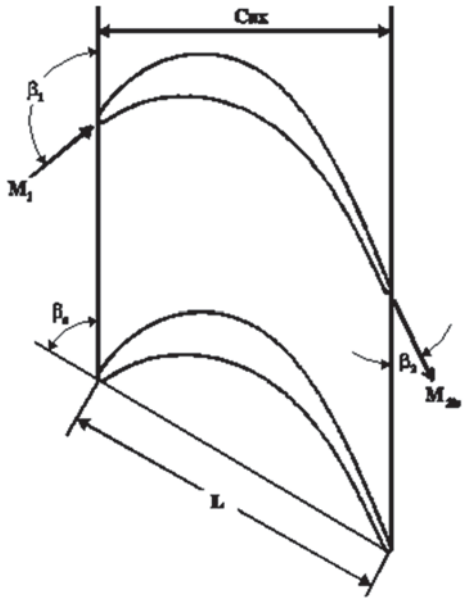

Fig. 1 T106A cascade geometry and nomenclature

III. OpenFOAM Framework

OpenFOAM is a CFD simulating toolbox consisting solvers, turbulence models and other applications unified in C++ libraries package. This open source package presents numerous advantages as being free, extensible, and object-oriented language construction rather than other commercial codes. This CFD software package was mainly developed by OpenCFD Ltd at ESI Group and distributed by the OpenFOAM Foundation [17].

IV. The Governing Equations and Turbulence Modeling

Considering the compressibility effects in the cascade flow, the Favre-averaged quantities are used by defining the relation

$$\tilde{\phi} = \overline{\rho\phi}/\overline{\rho} \tag{1}$$

where $\tilde{\phi}$ denotes Favre-averaged quantity, and $\overline{\rho}$ is Reynolds averaged density. Using definition (1), the Favre-averaged conservation equations of mass, momentum, and energy are written as [17]

$$\frac{\partial\overline{\rho}}{\partial t} + \frac{\partial(\overline{\rho}\tilde{u}_i)}{\partial x_i} = 0 \tag{2}$$

$$\frac{\partial(\overline{\rho}\tilde{u}_i)}{\partial t} + \frac{\partial(\overline{\rho}\tilde{u}_j\tilde{u}_i)}{\partial x_j} = -\frac{\partial P}{\partial x_i} + \frac{\partial(\overline{t}_{ji} + \tau_{ji})}{\partial x_j} \tag{3}$$

$$\frac{\partial(\overline{\rho}E)}{\partial t} + \frac{\partial}{\partial x_j}(\overline{\rho}\tilde{u}_j H) = \frac{\partial}{\partial x_j}\left[-q_{Lj} - q_{Tj} + \overline{t_{ji}u_i''} - \overline{\rho u_j''\frac{1}{2}u_i''u_i''}\right] + \frac{\partial}{\partial x_j}[\tilde{u}_i(\overline{t}_{ij} + \tau_{ij})] \tag{4}$$

where, u_i, P, u_i'', τ_{ij}, q_L, and q_T are instantaneous velocity components, mean static pressure, Favre fluctuating velocity components, Reynolds stress tensor, laminar, and turbulent mean heat flux vectors, respectively.

In (4), E and H are the total energy and total enthalpy, respectively, defined by

$$E = \tilde{e} + \frac{1}{2}\tilde{u}_i\tilde{u}_i \tag{5}$$

$$H = \tilde{h} + \frac{1}{2}\tilde{u}_i\tilde{u}_i \tag{6}$$

where e, k, and h are specific internal energy, specific enthalpy, and kinetic energy of turbulent fluctuations per unit mass, respectively. The viscous stress tensor $\overline{t}_{ij}$, strain rate tensor Sij, and laminar mean heat flux vector q_{Lj} are defined as

$$\overline{t}_{ij} = 2\mu\left(S_{ij} - \frac{1}{3}\frac{\partial\tilde{u}_k}{\partial x_k}\delta_{ij}\right) \tag{7}$$

$$S_{ij} = \frac{1}{2}\left(\frac{\partial\tilde{u}_i}{\partial x_j} + \frac{\partial\tilde{u}_j}{\partial x_i}\right) \tag{8}$$

$$q_{Lj} = -\kappa\frac{\partial\tilde{T}}{\partial x_j} \tag{9}$$

where κ is the thermal conduction coefficient. To close the governing equations, the ideal gas assumption is considered as

$$P = \overline{\rho}R\tilde{T} \tag{10}$$

and closure terms are modelled as

$$\tau_{ij} = \overline{-\rho u_i''u_j''} = 2\mu_T\left(S_{ij} - \frac{1}{3}\frac{\partial\tilde{u}_k}{\partial x_k}\delta_{ij}\right) - \frac{2}{3}\overline{\rho}k\delta_{ij} \tag{11}$$

$$q_{Tj} = \overline{\rho u_j''h''} = -\frac{\mu_T}{\mathrm{Pr}_T}\frac{\partial\tilde{h}}{\partial x_j} \tag{12}$$

$$\overline{t_{ji}u_i''} - \overline{\rho u_j''\frac{1}{2}u_i''u_i''} = \left(\mu + \frac{\mu_T}{\sigma_k}\right)\frac{\partial k}{\partial x_j} \tag{13}$$

In (11)-(13), μ_T and Pr_T are the eddy-viscosity and turbulent Prandtl number, respectively and would be defined according to the turbulence model.

Considering the inherent unsteadiness and the relatively low Reynolds number flows in LP turbines, the flow is transitional and tends to separate from aft part of the suction side of the blade. Consequently, the presence of the two mentioned factors limits the predictive capability of the RANS approaches for modelling of flow in highly loaded LP turbine cascades. For these reasons, in the present study, the flow simulation regarding the LP turbine cascade was carried out employing RANS and LES turbulence models. Moreover, the ability of LES model with respect to k-ε and k-ω models has been evaluated in predicting the flow characteristics, especially in shear layer regions.

A. Standard k-ε Model

From the turbulence point of view, standard k-ε model is the most dominantly used two-equation turbulence model which was initially suggested by Launder and Spalding (1974) [12]. In order to correlate the Reynolds stresses to the mean velocity gradients, the gradient hypothesis from Boussinesq (1877) has been applied, that relates the two mentioned parameters using the turbulent viscosity. Indeed, the transport equations for k and ε are written as

$$\frac{\partial(\rho k)}{\partial t} + \frac{\partial(\rho u_i k)}{\partial x_i} = \frac{\partial}{\partial x_i}\left[(\mu + \frac{\mu_T}{\sigma_k})\frac{\partial k}{\partial x_i}\right] + P_k - \rho\varepsilon \tag{14}$$

$$\frac{\partial(\rho\varepsilon)}{\partial t} + \frac{\partial(\rho u_i \varepsilon)}{\partial x_i} = \frac{\partial}{\partial x_i}\left[(\mu + \frac{\mu_T}{\sigma_\varepsilon})\frac{\partial\varepsilon}{\partial x_i}\right] + C_{\varepsilon 1}P_k\frac{\varepsilon}{k} - C_{\varepsilon 2}\rho\frac{\varepsilon^2}{k} \tag{15}$$

where the production term P_k is related to the strain rate, S, by

$$P_k = 4\mu_T S \tag{16}$$

$$S = \frac{1}{4}\left(f\frac{\partial u_i}{\partial x_j} + \frac{\partial u_j}{\partial x_i}\right)\frac{\partial u_i}{\partial x_j} \tag{17}$$

So, the eddy-viscosity relation in (18) is used to complete the

sets of the two equations

$$\mu_T = \rho C_\mu \frac{k^2}{\varepsilon} \tag{18}$$

B. Standard k-ω Model

The RANS equations are written in terms of mass-averaged variables and coupled with the low-Reynolds number k-ω turbulence model

$$\frac{\partial \rho}{\partial t} + \frac{\partial}{\partial x_j}(\rho u_j) = 0 \tag{19}$$

$$\frac{\partial (\rho u_j)}{\partial t} + \frac{\partial}{\partial x_j}(\rho u_j u_i) = -\frac{\partial p}{\partial x_i} + \frac{\partial \hat{\tau}_{ij}}{\partial x_j} \tag{20}$$

$$\frac{\partial (\rho U)}{\partial t} + \frac{\partial}{\partial x_j}(\rho u_j H) = \frac{\partial}{\partial x_j}\left[u_i \hat{\tau}_{ij} + (\mu + \sigma^* \mu_T)\frac{\partial k}{\partial x_j} - q_j \right] \tag{21}$$

$$\frac{\partial (\rho k)}{\partial t} + \frac{\partial}{\partial x_j}(\rho u_j k) = \tau_{ij}\frac{\partial u_i}{\partial x_j} - \beta^* \rho \omega k + \frac{\partial}{\partial x_j}\left[(\mu + \sigma^* \mu_T)\frac{\partial k}{\partial x_j} \right] \tag{22}$$

$$\frac{\partial (\rho \omega)}{\partial t} + \frac{\partial}{\partial x_j}(\rho u_j \omega) = \frac{\alpha \omega}{k}\tau_{ij}\frac{\partial u_i}{\partial x_j} - \beta \rho \omega^2 + \frac{\partial}{\partial x_j}\left[(\mu + \sigma \mu_T)\frac{\partial \omega}{\partial x_j} \right] \tag{23}$$

U and H are the specific total energy and enthalpy comprehensive of the TKE, k the eddy viscosity, μ_T is defined in terms of k and of the specific dissipation rate, ω according to the k-ω turbulence model of Wilcox [20]

$$\mu_T = \alpha^* \frac{\rho k}{\omega} \tag{24}$$

Inherently, the second model showed a better configuration of the flow and blade interactions. The wall functions included in this model allows receiving closer results, especially, in critical zones where the flow characteristics change unsteadily.

C. Large-Eddy Simulation (LES)

Generally, LES is a model between the DNS and the RANS. In LES, the interaction among large energetic structures, momentum, and energy transfer is filtered and the effect of the smallest scales of turbulence is just modeled.

The resolved eddies are obtained by a filtering operation (Leonard, 1974):

$$\overline{f}(x) = \int_\Omega f(x) G(x, x') dx' \tag{25}$$

where Ω is the entire domain, and G is a filter function which determines the size and structure of the small scales.

With respect to notations, the filtered conservation equations of mass and momentum for LES are as the same as RANS equations. However, energy equation has some differences and rewritten here as:

$$\frac{\partial (\overline{\rho}\tilde{E})}{\partial t} + \frac{\partial}{\partial x_j}\left[(\overline{\rho}\tilde{E} + \overline{p})\tilde{u}_j + \tilde{q}_{Lj} - \tilde{\sigma}_{ij}\tilde{u}_i \right] = -\frac{\partial}{\partial x_j}(\gamma C_v Q_j + \frac{1}{2}J_j - D_j) \tag{26}$$

where Q_j is the sub-grid scale (SGS) heat flux, defined and modeled by

$$Q_j = \overline{\rho}(\widetilde{u_j T} - \tilde{u}_j \tilde{T}) \approx -\frac{\overline{\rho}\nu_T}{\mathrm{Pr}_T}\frac{\partial \tilde{T}}{\partial x_j} \tag{27}$$

In (26), J_j is the SGS turbulent diffusion, and D_j is the SGS viscous diffusion which has the smallest value of the terms in the equation of total energy and is a very small fraction of the divergence of Q_j; hence, it is omitted from the energy equation.

As determined from the governing equations for LES, the only term to be determined is the SGS eddy viscosity $\mu_t = -\rho\nu_t$. Various models form simple dynamic Smagorinsky (1963) model to one- and two-equation models have been proposed by several researchers. Here, SA one-equation model was chosen due to its well behavior in wall-bounded and adverse pressure gradients flows in boundary layers [16].

In SA model, the eddy-viscosity is defined by

$$\mu_t = \overline{\rho}\hat{\nu} f_{\nu 1} \tag{28}$$

where f_{v1} is a constant, and $\hat{\nu}$ is obtained from transport equation

$$\frac{\partial}{\partial t}(\overline{\rho}\hat{\nu}) + \frac{\partial}{\partial t}(\overline{\rho}\tilde{u}_j\hat{\nu}) = S_p + D - S_D + S_t \tag{29}$$

where S_p is the production term, D is diffusion term, S_D is the dissipation term due to near-wall damping, and S_t is a source term.

V. Numerical Results

The present work comprises two distinct considerations of flow status on T106A cascade. The first phase belongs to the prediction of the separation region at a steady state flow condition over the blade. According to the specifications of both the flow and the blade, dealing with a separated flow is not beyond expectations.

To ensure the accurate region of the bubble occurrence, several operational factors affect. In fact, the concern is on removing the separation bubble away from the blade surface. The interaction between the rotor and stator rows leads to the wake entrance which is itself the result to vanish the bubble. The outlet-inlet proportion of the neighboring rows and the relative rotating frequency are of major influencing issues on the wake entrance to the cascade.

On the second phase, the focus is to study and simulate the wake effects on separated shear layer at unsteady working condition.

A. Steady State

As was mentioned, the flow field within subsonic LP turbine passages is subjected to a wide range of Mach numbers. Thus, a pressure-based algorithm is chosen in flow and thermal computations using OpenFOAM, as well. In order to select an appropriate solver, the computations have been performed with two different algorithms, pressure-based steady-state and unsteady time-marching strategy. The necessary boundary and initial conditions have been properly imposed on rhoSimplecFoam (steady-state) and rhoPimplecFoam (transient) solvers. The former is the compressible version of SIMPLE algorithm, while the latter is a combination form of compressible PISO and SIMPLE algorithms. The inlet condition was implemented to adjust exit Reynolds and isentropic Mach (M_{2is}) numbers indicated in Table I. Since the nature of flow near the trailing edge of the suction side is unsteady, test experiences considerably showed that the unsteady solver (rhoPimplecFoam) converged to a highly acceptable solution. Therefore, the numerical results illustrated through this work have been obtained by rhoPimplecFoam solver in accordance to the mentioned reasons**.** In order to avoid instability of errors, the Courant-Friedrichs-Lewy (CFL**)** has been kept below unity (1). The numerical results have been validated by surface pressure measurements reported by [3] and [6].

The pressure Coefficient is defined

$$Cp = \frac{P_{t1} - P}{P_{t1} - P_2} \tag{30}$$

where P_{t1}, P_1, and P_2 are denoted as the inlet total pressure, blade surface, and exit pressures, respectively.

The Mach number contours and streamline near the trailing edge are illustrated in Fig. 2. As it is seen, the flow rapidly turns and accelerates on the suction side and reaches to its maximum Mach number (*Ma*=0.7) before one third of surface length. On the other side, the flow turns and accelerates gradually and reaches to *Ma*=0.6 when leaving the cascade. Moreover, the generated vortices at trailing edge are depicted in Fig. 2.

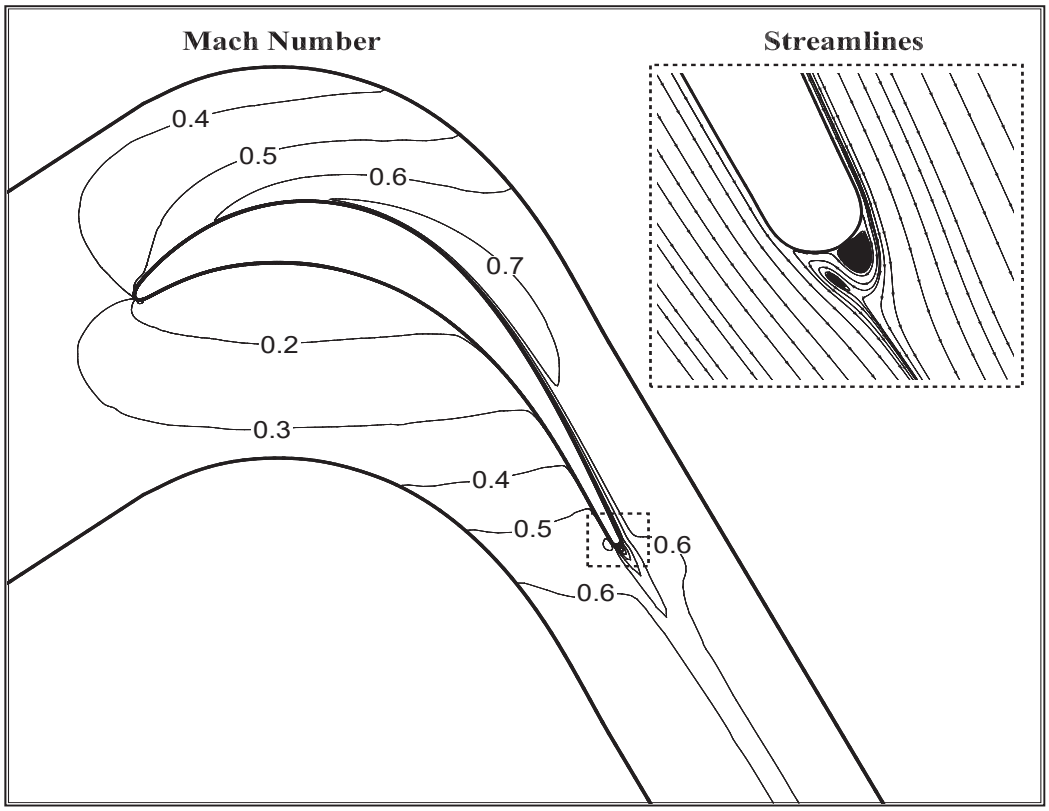

Fig. 2 Mach number contours of flow within cascade with design flow angle

In order to study the effects of grid resolution, the numerical simulation has been conducted on three sets of mesh resolutions. The different mesh densities from "1" to "3" are taken into consideration with the aim of predicting the most important feature of the dominant shear-layer through the mentioned LP turbine cascade, as separation bubble. Although the separation prediction was the main target to be computed at the initial phase, another feature named "pressure-Undershoot" positioned at the trailing edge of the pressure-side has been studied in parallel. The effects of grids on each of these two issues are interpreted through this article.

Grid numbers 1, 2, and 3 are used in all the three mentioned turbulence models, but the result of grid 3 is barely presented with LES model in the present work. Furthermore, through

meshes 1 and 2, the main concern is to study the pressure undershoot which is happening through computations as a commonplace numerical error since now. As is depicted in the pressure coefficient figures, the results from all the three turbulence models on grid 1 are considerably different from grid 2 showing a better pressure prediction at the trailing edge of the pressure side. Mesh densities are just increased in the shear-layer portion of the flow only for a better capturing the flow characteristics on the blade surfaces.

As can be seen in Figs. 3 and 4, k-ε model reveals a fairly good configuration of the *Cp* plot compared to the experiment. The two significant points are that this model shows remarkable deficiency in both capturing the separation bubble and the pressure prediction at the trailing edge of the airfoil.

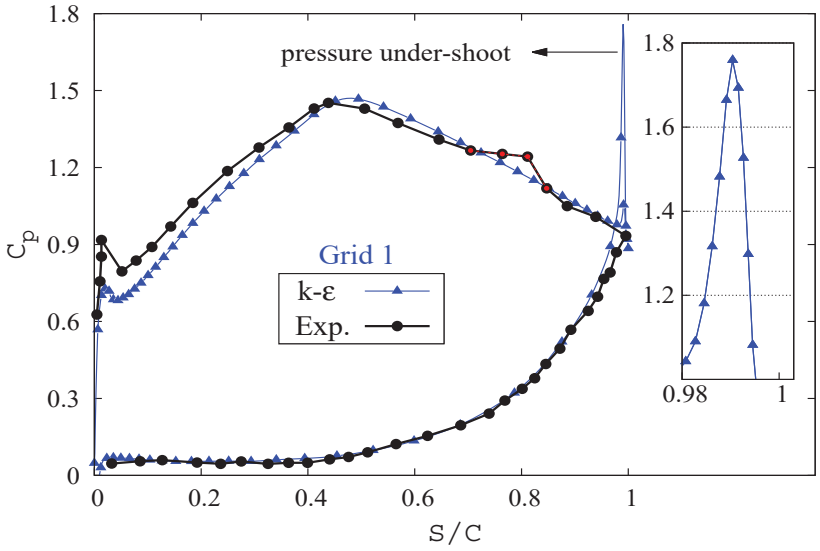

Fig. 3 Pressure distribution of grid 1 on k-ε model

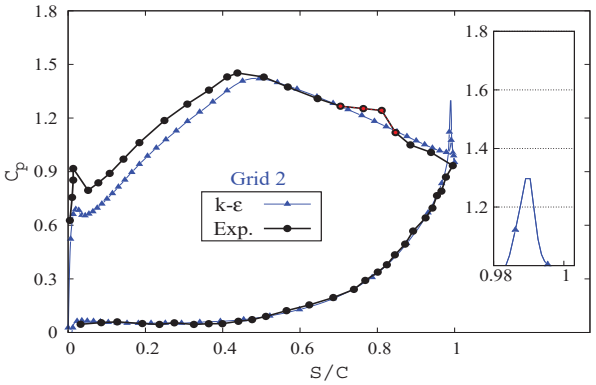

Fig. 4 Pressure distribution of grid 2 on k-ε model

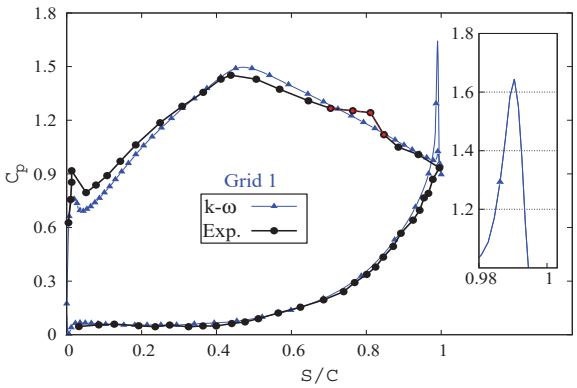

Fig. 5 Pressure distribution of grid 1 on k- ω model

Comparing the aforementioned figures with the relative results derived from the k-ω model in Figs. 5 and 6, it can easily be seen that the grid resolution from 1 to 2 had more influence in the k-ω model through better capturing the flow pressure especially when it exits from the cascade. The similarity that lays on both of these models is that neither of them were capable of predicting the separation over the rear side of the suction surface.

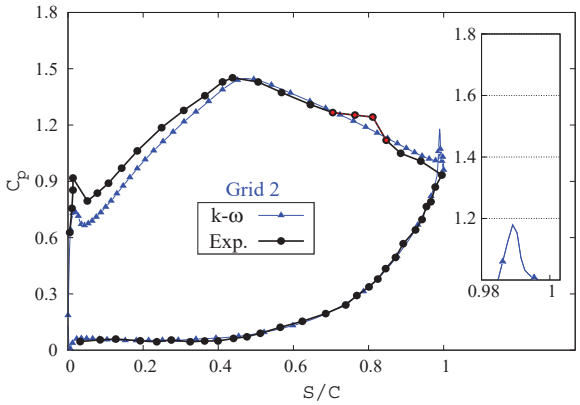

Fig. 6 Pressure distribution of grid 2 on k- ω model

The most efficient turbulence model in predicting the pressure distribution over the blade T106 in these simulations was the LES model. From Figs. 7 and 8, the effectiveness of implementing both LES turbulence model and a finer grid

resolution from 1 to 2 is obviously diagnosed. These effects are not only covering the pressure-undershoot around the end of the blade, but also an initial flow separation was predicted at this pace.

Even though the location and the size of the predicted bubble is rather different from what is compared with the Stieger and Hodson [2] experiment, but anyway this was very crucial to predict separation in steady simulation of the turbine working condition. Noticeably important, the deviations in the pressure calculations at the leading edge of the blade relate to non-exact inflow angle setting in experimental work [1].

Aside from the first RANS models, in accordance with the separation signs in the second mesh using LES model, attempts were taken to try this efficient model in a finer grid as well. Up to here, the pressure-undershoot became fairly comparable with what happens in a real state, and on the other hand, a sign of separation bubble is being predicted with a combination of LES model and the second grid. Hence, the grid number "3" was applied to this turbulence model for gaining a more accurate result compared to the experimental work.

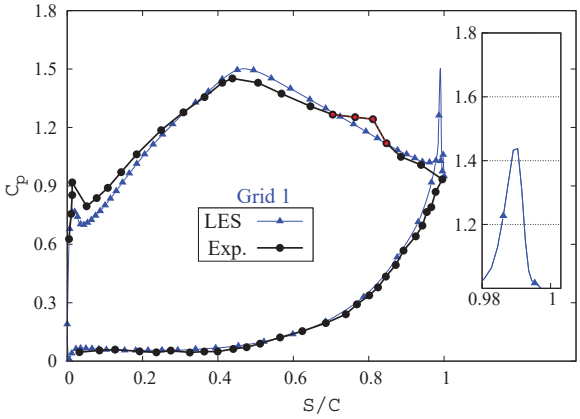

Fig. 7 Pressure distribution of grid 1 on LES model

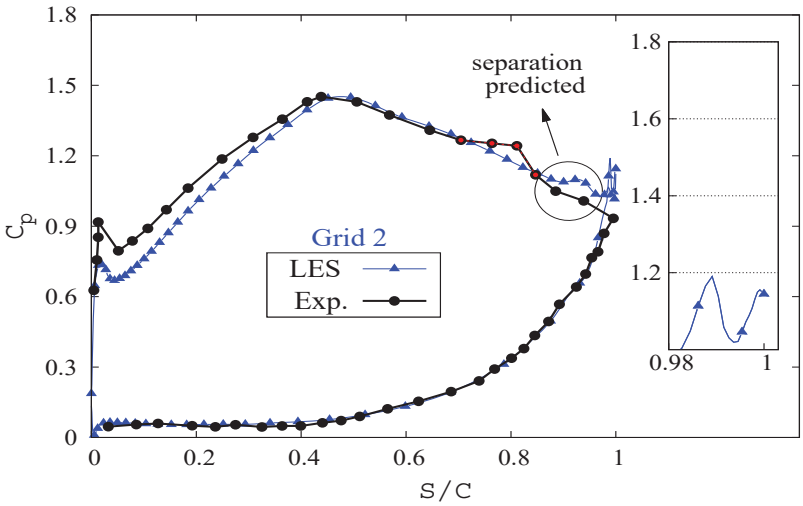

Fig. 8 Pressure distribution of grid 2 on LES model

Fig. 9 belongs to the LES model applied on the third and the finest grid structure. A reasonable harmony can be deduced from the comparisons of the numerical result extracted from LES model on the final grid and the experimental measurement data from Stieger and Hodson [3]. The separation bubble always reveals itself in a pressure plateau format in the pressure distributions plot.

As is declared with Stieger, the shear-layer separates from the suction surface at the position of 0.73 axial chord length and reattaches to the surface at 0.84 axial chord. Fig. 10 shows the surface friction computed on the suction wall of the blade. This plot exactly reveals that the separation bubble which is captured and shown in Fig. 9 is totally relevant with what was measured in experiments. The only difference between the simulation and the experiment remains on the bubble thickness over the blade surface which may be the result of numerous reasons through experimental tests and the numerical simulations.

Fig. 11 shows the shear layer separation at the mentioned location on the suction side of the blade in steady flow simulation. As is clear, the velocity vectors configure a rotational field which is mainly the occurrence of separation bubble.

B. Inflow Unsteadiness

In a real case of turbine passage, the interaction is indeed between the successive rotor and stator rows. In doing so, aside from the steady measurements of flow characteristics, considering the overall unsteady behavior of the flow field is being vitally significant. The dominant issue featuring in participating the rows interaction on each other is the wake emerging from the rotor and passing through the stator cascade. This wake results from the relative displacement of the two rows on the sliding interface in midway gap between the rows.

Because of the difference existing between the flow velocities near the suction and pressure surfaces of the cascade, the incoming wake attaches to the suction side, especially to the rear portion of the blade. Arising from the inherent structure of a wake, it imposes two distinct disturbances to the suction side

shear layer. These are known as large and small scale disturbances. The former induces negative jet impingements perpendicularly towards the suction surface which lead to a higher level unsteadiness by creating vertical structures and Kelvin-Helmholtz instability.

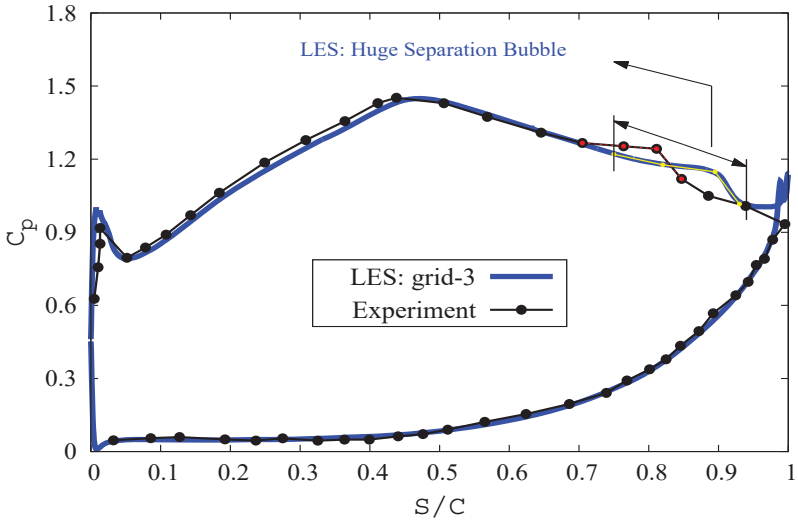

Fig. 9 Pressure distribution of grid 3 on LES model

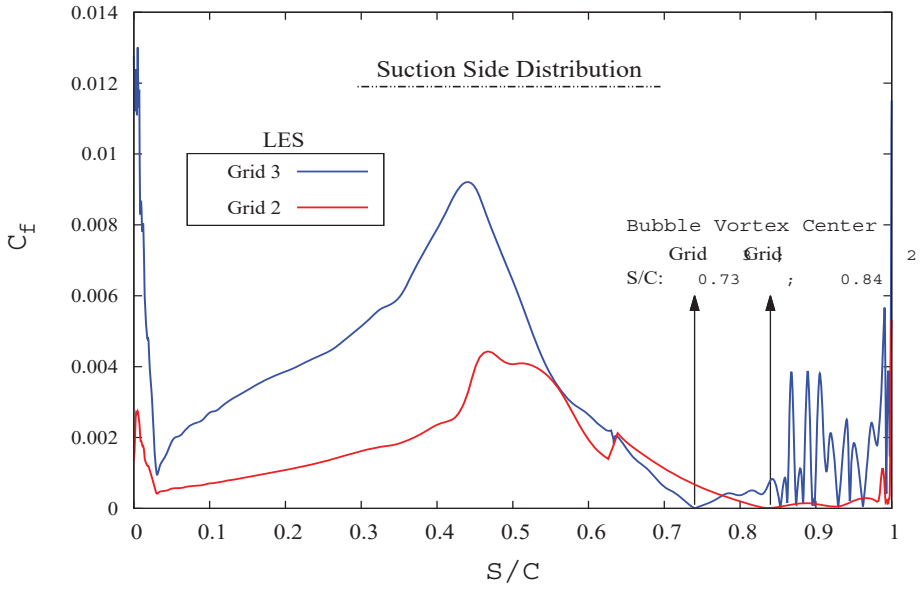

Fig. 10 Surface friction coefficients on grids 2 and 3 using LES model

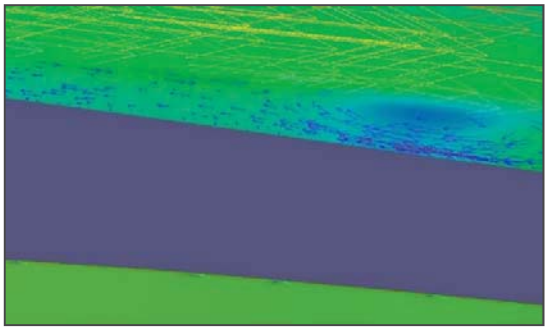

Fig. 11 Suction side separation bubble in steady flow measurements

Functionality, small scale disturbances cause the separated layer to reattach to the surface by compensating energy loss and aligning the vertical structures toward the passing flow field direction, specifically in the shear layer.

Because of the aforementioned details, Opoka et al. [6] aimed to set up the same experiment as Stieger and Hodson [3] except in transmitting the whole wake to the cascade flow. Inspired from Roach [21] work, they used a turbulence grid at cascade inlet to import small scale disturbances. Fig. 12 shows a typical turbulence grid at the inlet upstream used by Opoka et al. [6] in their tests to pass the flow.

Fig. 12 Typical schematic turbulence grid used in experiments

The control mechanism of transmitting a wake to the cascade in the experiment of Stieger et al. [3] was the changes in the proportion of flow exit patch length in previous row (S_b) to the inlet length of the current cascade (S_c). They correlated this proportion (S_b/S_c) to frequency which represents the interaction intervals of the two successive rows. The frequency value of 0.68 belongs to a proportion, which leads to the entrance of a complete wake to the cascade from the leading to trailing edges of the blade. In this unsteady condition, the flow shear layer revealed to be attached to the suction surface in the experiment of Stieger et al. [3].

Due to a different strategy of Opoka et al. [6] in inducing unsteady effects compared to steady tests, they managed to introduce another parameter known as free stream turbulence intensity (FSTI) that represents the value of turbulence intensity. Opoka et al. probed the flow turbulence intensity directly at the inlet location of the cascade. Similar to the 0.68 frequency value in Stieger et al. [3] work, FSTI value equal to 4% was the condition which led to quell the separated shear layer in the regions between 0.63 to 0.9 of S/S_c values.

In the present CFD Simulation, a new technique was employed concerning with importing disturbances to the cascade entry. At the initial condition of the simulation, the velocity value is set with a turbulent-Inlet condition which varies the velocity vectors from cell to cell. This was the way to apply different velocity vector magnitudes (see Fig. 13) at the inlet patch of the cascade. In accordance with the relevant experiment [6], in the current CFD study, the disturbance or FSTI value is set to 4% to resemble a fair situation of the wake presence and its major effects as small scale disturbances.

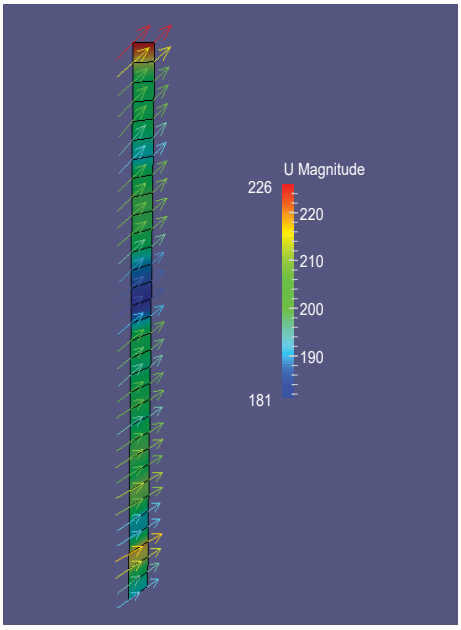

Fig. 13 Instant velocity magnitudes applied at the simulation inlet

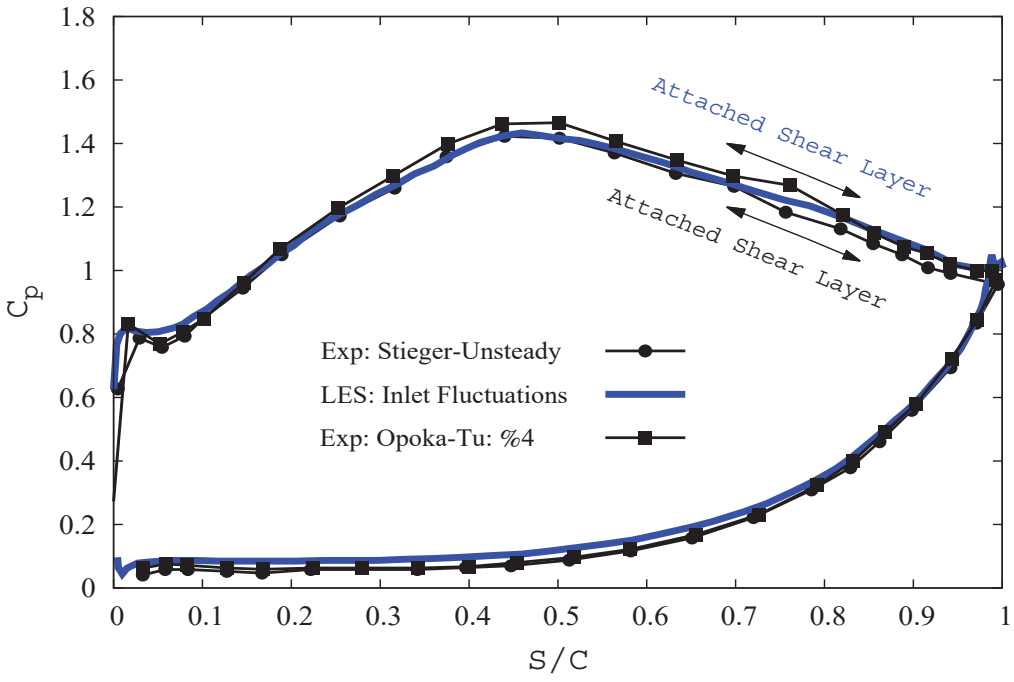

Fig. 14 Comparison of separation bubble disappearance in LES with experiments [3] and [6]

As is shown in Fig. 14, the comparison of the current result with those of mentioned experiments [3] and [6] reveals the same status of flow separation bubble region which has become attached to the suction surface corresponding to presence of the wake or its effects.

This achievement is remarkably important in numerical investigations. Instead of simulating a complete wake as unsteady flow, the same results are gained in a more efficient approach. Both the time and CPU costs of the current simulation reduce considerably in applying the unsteadiness rather than the unsteady wake.

VI. Conclusion

The effects of both steady and unsteady flow field are numerically simulated in a highly-loaded LP turbine cascade. Firstly, the attempts were to predict the location of separation bubble in a steady flow status. Among all three turbulence models and grid structures, LES model on grid 3 was the most appropriate condition to accurately capture the separated shear layer. Second phase was to simulate the flow behavior in an unsteady condition to further investigate its effects on the separated flow. Inspired from the experiments of Opoka et al. [6], in order to see the wake effects on flow separation, the main key is just to apply the small-scale disturbances which originate from the oncoming wake. The implemented approach to simulate the mentioned unsteadiness rather than to import the wake worked efficiently in this numerical study. Both in the first and the second phase of the current study which deals with steady and unsteady flow conditions, a fair agreement is seen in comparing the results with those of experiments as well.

References

[1] Hodson, H.P. and Howell, R.J., "Bladerow Interactions, Transition, and High-Lift Aerofoils in Low-Pressure Turbines," *Annual Review of Fluid Mechanics*, vol. 37, pp. 71-98, 2005.

[2] Stieger, R. and Hodson, H.P., "The Transition Mechanism of Highly Loaded LP Turbine Blades," *Journal of Turbomachinery-Transactions of ASME*, vol. 126, No. 4, pp. 536-543, 2004.

[3] Stieger, R. and Hodson, H.P., "The Unsteady development of a Turbulent Wake Through a Downstream Low-Pressure Turbine Blade Passage," *Journal of Turbomachinery-Transactions of ASME*, vol. 127, pp. 388-394, 2005.

[4] Lodefier, K. and Dick, E., "Modeling of Unsteady Transition in Low Pressure Turbine Blade Flows with Two Dynamic Intermittency Equations," *Flow, Turbulence and Combustion*, vol. 76, pp. 103–132, 2005.

[5] Wissink, J.G., Rodi, W., and Hodson, H.P., "The Influence of Disturbances Carried by Periodically Incoming Wakes on the Separating Flow Around a Turbine Blade," *Int. J. Heat and Fluid Flow*, vol. 27, pp. 721-729, 2006.

[6] Opoka M.M., Thomas, R.L., and Hodson H.P., "Boundary Layer Transition on the High Lift T106A Low-Pressure Turbine Blade with an Oscillating Downstream Pressure Field," *Journal of Turbomachinery-Transactions of ASME*, vol. 130, No. 2, Article number 021009, 2008.

[7] Calzada, P.D.L., and Alonso, A., "Numerical Investigation of Heat Transfer in Turbine Cascades with Separated Flows," *Journal of Turbomachinery-Transactions of ASME*, vol. 125, no. 2, pp. 260–266, 2003.

[8] H. P. Hodson and R. G. Dominy, ASME J. Turbomach. 109, 201 (1987).

[9] X. Wu and P. A. Durbin, "Evidence of longitudinal vortices evolved from distorted wakes in a turbine passage," *J. Fluid Mechanics*, vol. 446, P. 199–228, 2001.

[10] V. Michelassi, J. G. Wissink, J. Fröhlich, and W. Rodi, "Large-eddy simulation of flow around low-pressure turbine blade with incoming wakes," *AIAA J.*, vol. 41, no. 11, P. 2143–2156, 2003.

[11] K. Matsuura and C. Kat, "Large-eddy simulation of compressible transitional flows in a low-pressure turbine cascade," *AIAA J.*, vol. 45, no. 2, P. 442–457, 2007.

[12] C. Velez, P. Coronado, H. Al-Kuran, and M. Ilie, "Numerical computations of turbine blade aerodynamics; comparison of LES, SAS, SST, SA, and k-ε," AIAA/ASME/SAE/ASEE Joint Propulsion Conference & Exhibit, 2011.

[13] A. Ghidoni, A. Colombo, S. Rebay, and F. Bassi, "Simulation of the transitional flow in a low pressure gas turbine cascade with a high-order discontinuous galerkin method," *ASME Journal of Fluids Engineering*, Vol. 135, No. 7, P. 071101-1–071101-8, 2013.

[14] R., E. Mayle, "The Role of Laminar-Turbulent Transition in Gas Turbine Engines," *J. Turbomachinery*, vol. 113, no. 4, pp. 509-536, 1991.

[15] M. Stieger, W. Richtering, J. S. Pedersen, and P. Lindner, "Small-angle neutron scattering study of structural changes in temperature sensitive microgel colloids," *The Journal of chemical physics*, vol. 120, no. 13, pp.6197-6206, 2004.

[16] OpenFOAM project web pages http://www.openfoam.com, accessd 01/04/2014.

[17] Cobley, K., Coleman, N., Siden, G., Arndt, N., 1997, "Design of new three stage low pressure turbine for BMW Rolls-Royce BR715 engine", ASME 97-GT-419.

[18] Hoheisel, H., "Test Case E/CA-6, Subsonic Turbine Cascade T106, Test Cases for Computation of Internal Flows in Aero Engine Components," AGARD-AR-275, 1990.

[19] T. Hildebrandt and L. Fottner, "A numerical study of the influence of grid refinement and turbulence modeling on the flow field inside a highly loaded turbine cascade," *J. Turbomachinery*, vol. 121, no. 4, pp. 709–716, 1999.

[20] David C Wilcox, *Turbulence Modeling for CFD*, 3rd ed. DCW Industries, Inc., 2006, 522 pages.

[21] Roach, P. E., 1987, "The Generation of Nearly Isotropic Turbulence by Means of Grids," Int. J. Heat Fluid Flow, 8(2), pp. 82–92.